Int. J. Electrochem. Sci., 16 **(2021)** Article ID: 210261, doi: 10.20964/2020.12.20

International Journal of
ELECTROCHEMICAL
SCIENCE
www.electrochemsci.org

Short Communication

Effect of Extrusion Direction on Microstructure and Corrosion Behavior of Rare Earth doped AZ91 Alloy

Xiaoyu Fu[1], *Ruiling Jia*[1,*], *Feng Guo*[1], *Wen Ma*[1], *Huixia Zhang*[2], *Jian Hou*[2]

[1] Inner Mongolia Key Laboratory of Thin Film and Coatings, School of Materials Science and Engineering, Inner Mongolia University of Technology
[2] State Key Laboratory of marine corrosion and protection, 725 Research Institute of China Shipbuilding Industry Corporation, Qingdao 266101
[*]E-mail: jrl014014@163.com

Received: 1 August 2020 / *Accepted:* 20 September 2020 / *Published:* 31 December 2020

By studying the changes in the grain size of α-Mg matrix, the distribution and size of the intermetallic phases in the transverse and longitudinal sections of the extruded AZ91 alloy with 1.0% (La, Ce) mischmetal (MM) addition, in combination with the corrosion behavior on the transverse and longitudinal sections, the corrosion mechanism of them caused by the change of microstructure was revealed. The results showed that a grain refinement and size reducing in β-$Mg_{17}Al_{12}$ and Al_4(La, Ce) phases had been found in extruded alloy. The relative potential difference of the intermetallic phases was influenced by extrusion process, the one between the Al_4(La, Ce) phase and Mg matrix in the longitudinal section of the extruded alloy is the highest, but Al_4(La, Ce) phase was a weak cathode. The decrease in the size of β-$Mg_{17}Al_{12}$ reduced the area of the cathode of the micro-galvanic coupling, the change of the size of Al_4(La, Ce) phase has no remarkable effect on the micro-galvanic corrosion behavior. Corrosion morphologies were varied with difference in extrusion direction, the corrosion morphology in the transverse section is mainly pitting corrosion caused by the cathode phases of β-$Mg_{17}Al_{12}$ and individual Al_4(La, Ce). The corrosion morphology in the longitudinal section are characterized by corrosion streamline parallel to extrusion direction, the corrosion occurs at the grain boundaries of the recrystallized grain.

Keywords: Magnesium Alloy; Rare earth; Extrusion; Corrosion

1. INTRODUCTION

Mg alloy is known as the green engineering material in the 21st century, but their actual usage is limited due to the low strength and insufficient corrosion performance [1]. Hence, some methods are required to improve the range of properties of Mg alloy [2-3]. In this case, domestic and foreign scholars are paying more and more attention to the application research of Mg alloy. Research shows that the original microstructure of Mg alloy can be changed by heat treatment, forming, rare earth alloying, which has obvious effect on the corrosion resistance of Mg alloy. Aung [4] reported that when the grain size of the alloy was relatively small, the volume fraction of grain boundaries increased and acted as a barrier to hinder the corrosion propagation. Li [5] analyzed the effects of microstructure evolution during T4 treatment on the corrosion resistance of Mg-Zn-Y alloys and believed that the dissolution of W-phase under T4 treatment condition could improve the corrosion resistance of the alloy. Wang [6] revealed that the corrosion resistance of Mg-Gd-Zn (Al) alloy was remarkably improved due to the precipitation of the long-period stacking ordered (LPSO) phase by T6 treatment. Some studies believed that hot extrusion processes could cause dynamic recrystallization, thereby achieving the refinement of grain size and improved mechanical properties [7-10]. Chen [11] analyzed that the addition of rare earth La or Ce could increase the density of the corrosion product film, therefore improving the protection of the film to the Mg alloy. Birbilis [12] found that the grains of the pure Mg could be greatly refined by equal channel angular pressing (ECAP), corrosion current density reduced with decreasing grain size. Hamu [13] studied the influence of the microstructure change on the corrosion behavior of Mg alloy after large plastic deformation. By comparing conventional extrusion and equal channel angular extrusion (ECAE) on as-cast AZ31 alloy, it was found that the changes of the microstructure after ECAE deformation were mainly manifested as grain refinement and increased dislocation density. It is well known that the micro-galvanic corrosion is a common corrosion type in the Mg alloys. It has been widely accepted that local galvanic coupling can be present in the microstructure of Mg alloy due to the intermetallic phases with higher potential than that of the matrix. The existence of the galvanic coupling can induce initiation sites of localized corrosion because the intermetallic phase always acts as cathodes [14-16]. Blu [17] found that the corrosion attack to the matrix of the AZ91D alloy was affected by the Volta potential of β-$Mg_{17}Al_{12}$ phase relative to the matrix. The study of Zhao [18] reported the potential of the large granular β phase independently distributed in the AZ91 alloy was higher than that of the adjacent matrix, so they formed a corrosion galvanic coupling and increased the localized corrosion of the AZ91 alloy.

Regarding the research on the corrosion mechanism of Mg alloy, most researches have observed and discussed the influence of single factor. There is little research on the effect of extrusion deformation on the corrosion rules of the Mg alloy containing rare earth. In order to clarify the extrusion deformation on the effect of the corrosion mechanism of the AZ91 alloy containing (La, Ce) MM, in present work, the corrosion behavior on the transverse and longitudinal sections of the extruded AZ91 alloy with 1.0% (La, Ce) MM was studied.

2. EXPERIMENT

The experimental materials used in this work were semi-continuous casting AZ91 alloy ingot with 1.0% (La, Ce) MM addition. The chemical composition was shown in Table1.The Mg alloy was machined into cylinder specimens with the size of Φ 40 × 50 mm by wire electric discharge machining (WEDM). The cylinder specimens were homogenized in a resistance furnace with the holding temperature of 380 ℃ for 12h, in order to reduce the phenomenon of dendrite and segregation in semi-continuous casting Mg alloy. The homogenized Mg alloy was extruded in a metal mold with a Φ9 mm opening. The extrusion parameters were as follows: extrusion temperature was 380 ℃, extrusion speed was 45 mm/min. The samples were intercepted along the perpendicular and parallel to the extrusion direction, called the transverse section and the longitudinal section, respectively.

Table 1. Chemical composition of AZ91 alloy with 1.0% (La, Ce) MM (wt.%)

Alloy	Elements					
	Al	Zn	Mn	Fe	La	Ce
AZ91+1.0% (La, Ce)	9.69	0.78	<0.05	0.007	0.400	0.750

After mechanical grinding and polishing, some samples was corroded with picric acid. The changes of the grain size of the AZ91 Mg alloy with 1.0% (La, Ce) MM were observed by optical microscope (Axio Imager.A1m, Germany) before and after extrusion. The composition, size change and distribution of intermetallic phase in the alloy were inspected by scanning electron microscope (SEM, Sigma500, Germany). Scanning probe microscope (SKPFM, MultiMode8, America) was employed to test the relative potential difference between the intermetallic phase and the matrix, in order to analyze the influence of the phase size change on the relative potential difference. The corrosion morphology of Mg alloy before and after extrusion was observed by the above SEM. Electrochemical atomic force microscope (ECAFM, MultiMode8, America) was used to in situ observe the corrosion morphology of intermetallic phase and analyze the effect of extrusion on the corrosion mechanism of the Mg alloy.

3. RESULTS AND DISCUSSION

3.1 Microstructure of Mg alloy before and after extrusion

The microstructure of the AZ91 alloy with 1.0% (La, Ce) MM before and after extrusion is shown in Fig. 1. It can be seen from Fig. 1(a) that the microstructure of semi-continuous casting Mg alloy is characterized by big size grains, dendrites β-$Mg_{17}Al_{12}$ phase distributed along the grain boundaries, and scattered needle-like intermetallic phase. In our previous work [19], it was reported that the needle-like phases were Al_4(La, Ce) phase. After homogenization treatment, dendrites β-$Mg_{17}Al_{12}$ phase reduced and grain boundaries become thinner, leaving needle-like Al_4(La, Ce) phase (Fig. 1(b)). (c) and (d) in Fig. 1 show that the grain size of the extruded Mg alloy is obviously reduced and the grain boundary is refined. The grain size is about 5μm and more uniform in the transverse section (Fig. 1(c)). Large number of dynamic recrystallized grains are distributed inside and around the grain boundary in the longitudinal section, the grain size is not uniform. The smaller grain is about 2-3μm and the larger one is about 10μm. The dynamic recrystallization grains are mostly distributed around the smaller grains (Fig. 1(d)).

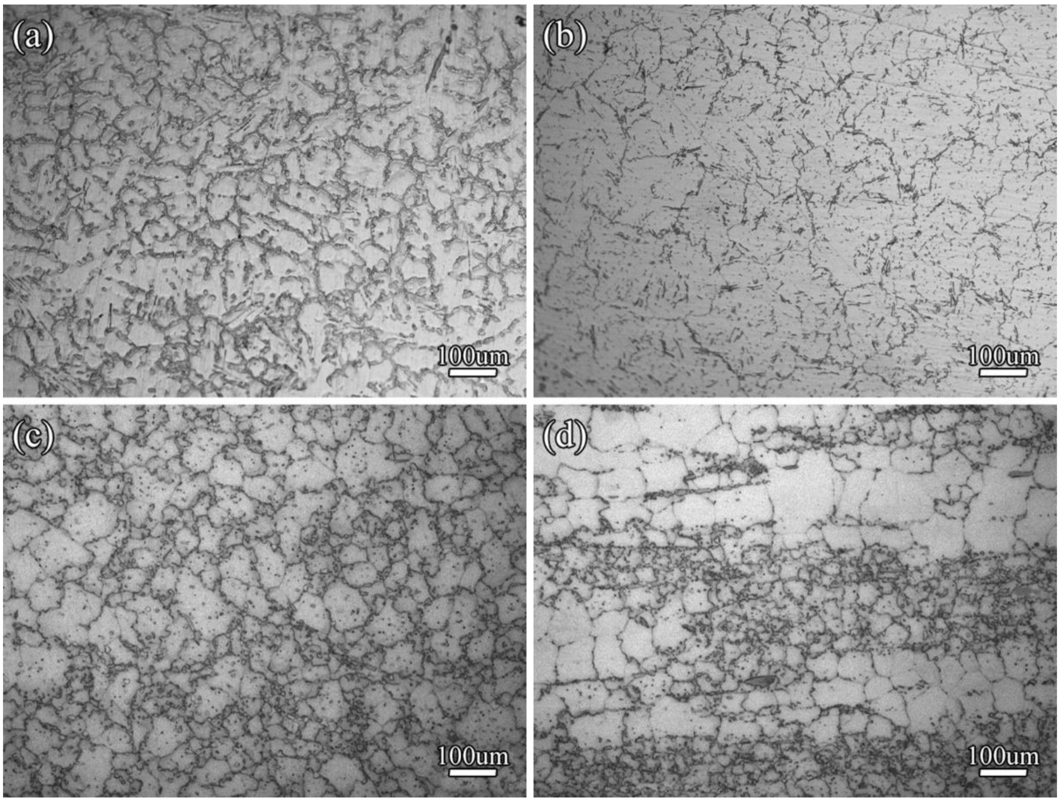

Figure 1. Microstructure of AZ91+1.0% (La, Ce) alloy (a) semi-continuous as-cast, (b) homogenization treatment, (c) transverse section after extrusion, (d) longitudinal section after extrusion.

The morphology of the AZ91 alloy with 1.0% (La, Ce) MM before and after extrusion is presented in Fig. 2. According to the phase shape, the dark gray part is matrix, the light gray is β-$Mg_{17}Al_{12}$ phase, and the bright white is Al_4(La, Ce) phase. It can be seen from Fig. 2(a), the β-$Mg_{17}Al_{12}$ phase exists in a discontinuous network structure, and Al_4(La, Ce) phase distributes in the matrix. After homogenization, the β-$Mg_{17}Al_{12}$ phase is obviously refined because part of them have dissolved, the size and morphology of the Al_4(La, Ce) phase have not changed because it is relatively stable (Fig.2(b)). According to Figs. 2 (c) and (d), the size of the β-$Mg_{17}Al_{12}$ phase and the Al_4(La, Ce) phase in the transverse section of the extruded Mg alloy are mostly smaller than 1μm, uniformly distributed in the matrix (Fig. 2(c)), Zhu [20] had studied the effects of extrusion passes on the microstructure and mechanical properties of the AZ31-Ce Mg alloy prepared by solid-phase synthesis**.** The results showed that the second phase was constantly crushed and deformed, and finally exhibited a granulated shape with the number of extrusion passes increasing. However, in the longitudinal section of the extruded Mg alloy, the most of β-$Mg_{17}Al_{12}$ phase and Al_4(La, Ce) phase are distributed along the extrusion direction, and a few of them are independently distributed on the matrix. The size of the intermetallic phases is mostly the same as that in the transverse section, and there are a few intermetallic phases with larger size in the longitudinal section (Fig. 2(d)). This typical morphology was also reported by Zeng [21], after extrusion deformation, the second phase presents a strip distribution along the parallel direction to the extrusion.

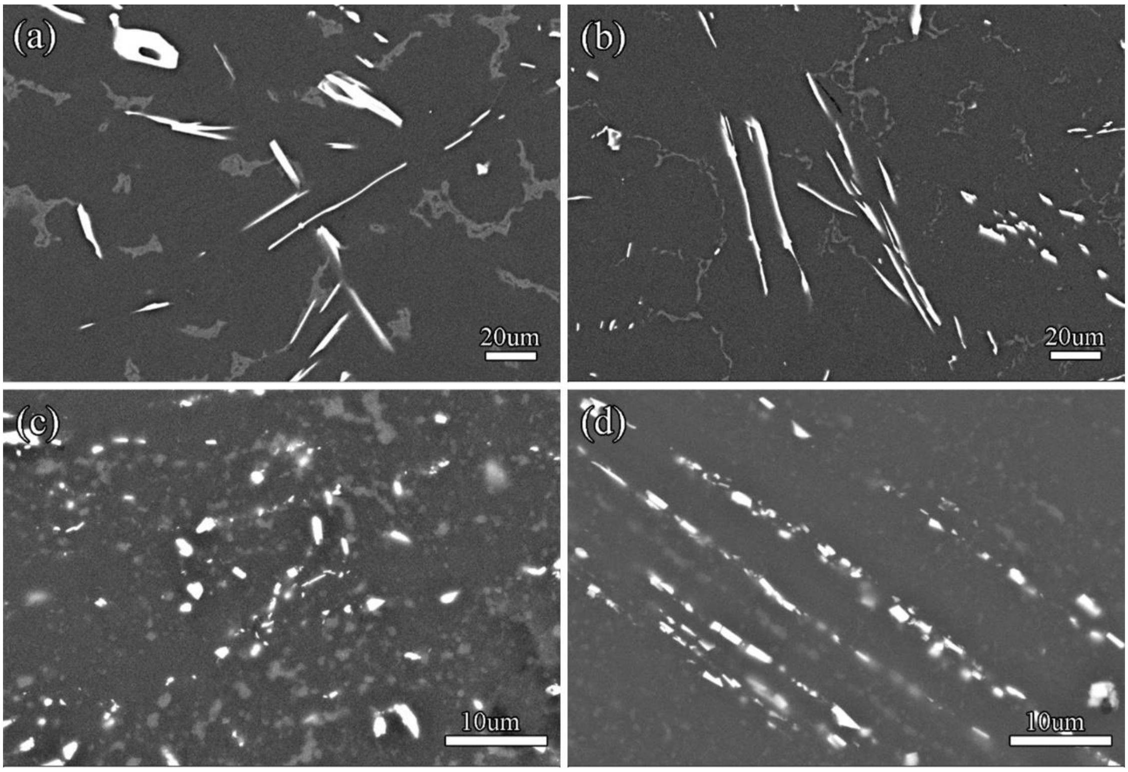

Figure 2. SEM morphologies of AZ91+1.0% (La, Ce) (a) semi-continuous as-cast, (b)homogenization treatment, (c) transverse section after extrusion, (d) longitudinal section after extrusion.

3.2 SKPFM potential measurement

Extrusion deformation can change the size and distribution of the phases. In order to further explore the effect of the relative potential difference between the phases on the micro-galvanic corrosion of the Mg alloy, the potential mapping of the AZ91 alloy with 1.0% (La, Ce) MM before and after extrusion was measured. 3D potential mapping and line-profile analysis are shown in Fig. 3. The results of the relative potential difference between the intermetallic phase and the matrix are listed in Table 2. The relative potential difference between the β-$Mg_{17}Al_{12}$ phase and the matrix is 110-150 mV for the semi-continuous casting Mg alloy. After homogenization, the relative potential difference between them decreased to 100-130 mV. After extrusion, the relative potential difference between them in the transverse section is 130-200 mV. It is obviously increased in the longitudinal section, reaching to 300-400 mV. The relative potential difference between the Al_4(La, Ce) phase and matrix is 300-370 mV for the semi-continuous casting Mg alloy. After homogenization, the relative potential difference of them is slightly reduced to 300-350 mV. After extrusion, the potential difference between them has no obvious change in the transverse section. But in the longitudinal section, the relative potential difference between the Al_4(La, Ce) phase and matrix is greatly improved and varies with the size of the Al_4(La, Ce) phase. The relative potential difference of the Al_4(La, Ce) whose size up to 1μm reaches 410-440 mV and whose size 1-2 μm reaches 470-520 mV. It can be concluded from the above results that the relative potential difference between β-$Mg_{17}Al_{12}$ phase, Al_4(La, Ce) phase and the matrix increases after extrusion.

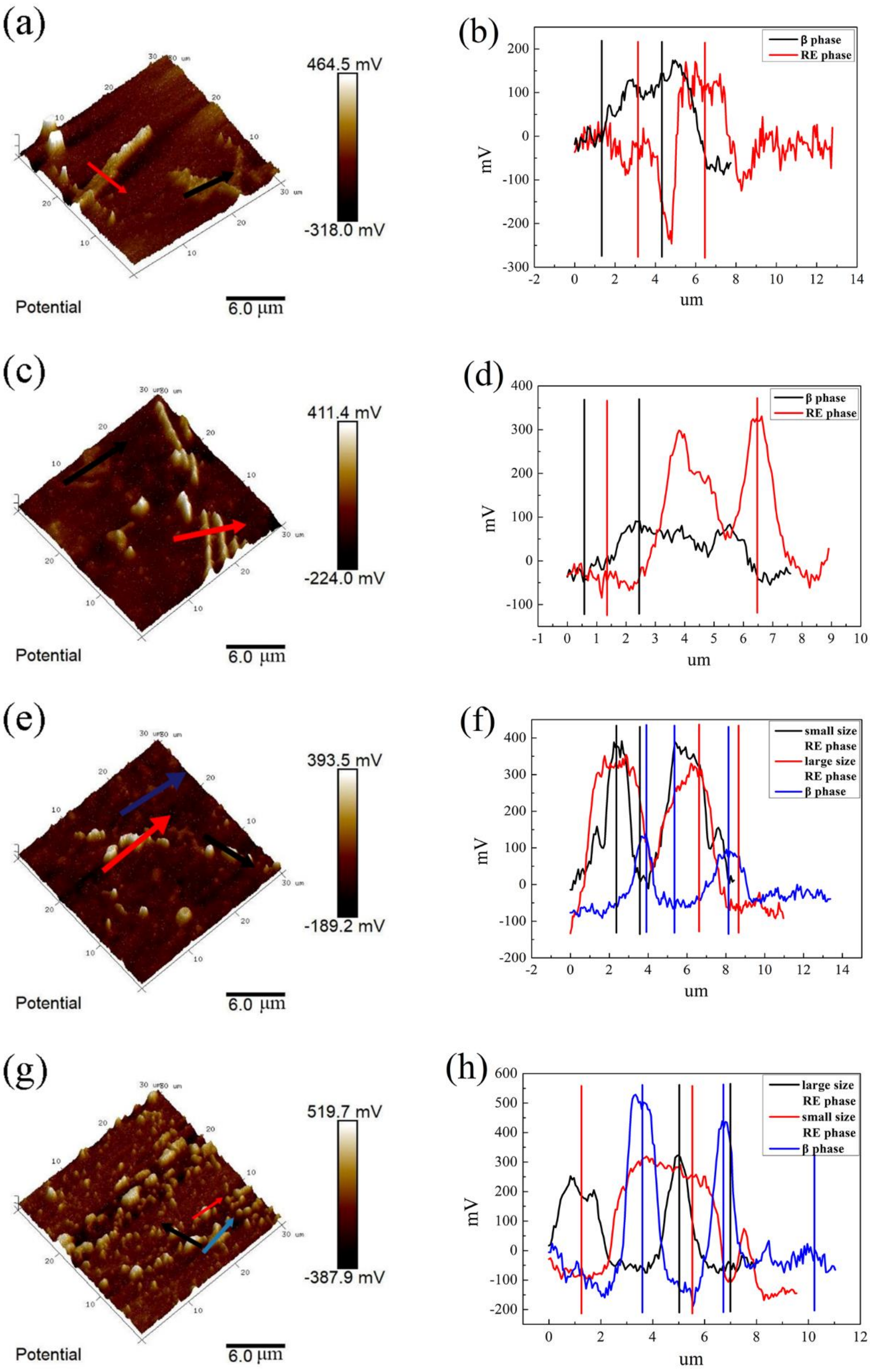

Figure 3. 3D potential mapping and line-profile analysis of AZ91+1.0% (La, Ce) alloy: (a)(b) semi-continuous as-cast, (c)(d) homogenization treatment, (e)(f) transverse section after extrusion, (g)(h) longitudinal section after extrusion.

Table 2. The relative potential difference between intermetallic phases and matrix in the AZ91 alloy with 1.0% (La, Ce) MM before and after extrusion

Alloy	Condition	Size of β phase (μm)	Potential difference (mV)	Size of rare earth phase (μm)	Potential difference(mV)
Before extrusion	Semi continuous casting	2-10	110-150	2-5	300-370
	Homogenization treatment	2-5	100-130	2-5	300-350
After extrusion	Transverse section	≤1	180-200	≤1	320-370
		1-2	130-150	1-2	300-370
	Longitudinal section	≤1	360-400	≤1	410-440
		1-2	300-380	1-2	470-520

3.3 Corrosion Morphology Characterization

In order to investigate the effect of intermetallic phase in the AZ91 alloy with 1.0% (La, Ce) MM addition, the in-situ observation on corrosion morphology of Mg alloy immersed in 0.1 mol/L NaCl solution was carried out. Fig. 4 shows the corrosion morphology of the intermetallic phase immersed in 0.1 mol/L NaCl solution for 5 min and 35 min. It can be seen from Fig. 4(a) that the edge of needle like Al_4(La, Ce) phase is clear without any corrosion after immersion for 5 min. A small amount of corrosion products is evident along the edge of the needle like phase after 35 min of immersion (Fig. 4(b)), indicating that slightly corrosion has occurred at the interface between the Al_4(La, Ce) phase and the matrix. But no obvious corrosion attack has been seen at the matrix adjacent to the Al_4(La, Ce) phase, which illustrates that the Al_4(La, Ce) phase do not exert a significant effect on the micro-galvanic corrosion of the semi-continuous as-cast AZ91 alloy. Figs. 4 (c) and (d) show the size of intermetallic phase in the transverse section of the extruded alloy greatly decreases. Compared to the corrosion morphologies of 5 min and 35 min immersion, there is no significant difference between them (circle-marked places). This indicates that Al_4(La, Ce) phase in the transverse section of the extruded alloy do not present the micro-galvanic corrosion with Mg matrix. Figs. 4 (e) and (f) show that corrosion morphologies of the Al_4(La, Ce) phase in the longitudinal section of the extruded alloy, after 5 min of immersion, corrosion products on the surface of the Al_4(La, Ce) phase can be seen. 30 minutes later, there is no obvious change on the surface of the Al_4(La, Ce) phase. Their common feature is the distribution of the corrosion products along the extrusion direction, which is not typical corrosion morphology of the micro-galvanic corrosion. According to SKPFM measurements (see Table 2), the relative potential difference between the Al_4(La, Ce) phase and Mg matrix in the longitudinal section of the extruded alloy is the highest (410-440 mV or 470-520 mV). According to the in-situ ECAFM observation, it is found that the Al_4(La, Ce) phases with the highest potential difference relative to the matrix do not exert significantly galvanic effect. This contradictory result has been explained by Hurley

[22], they believed that SKPFM had utility as a method to provide expected corrosion and micro-galvanic corrosion behavior, they are insufficient for determining whether the phase was an effective cathode or anode because a potential is not an index to kinetics.

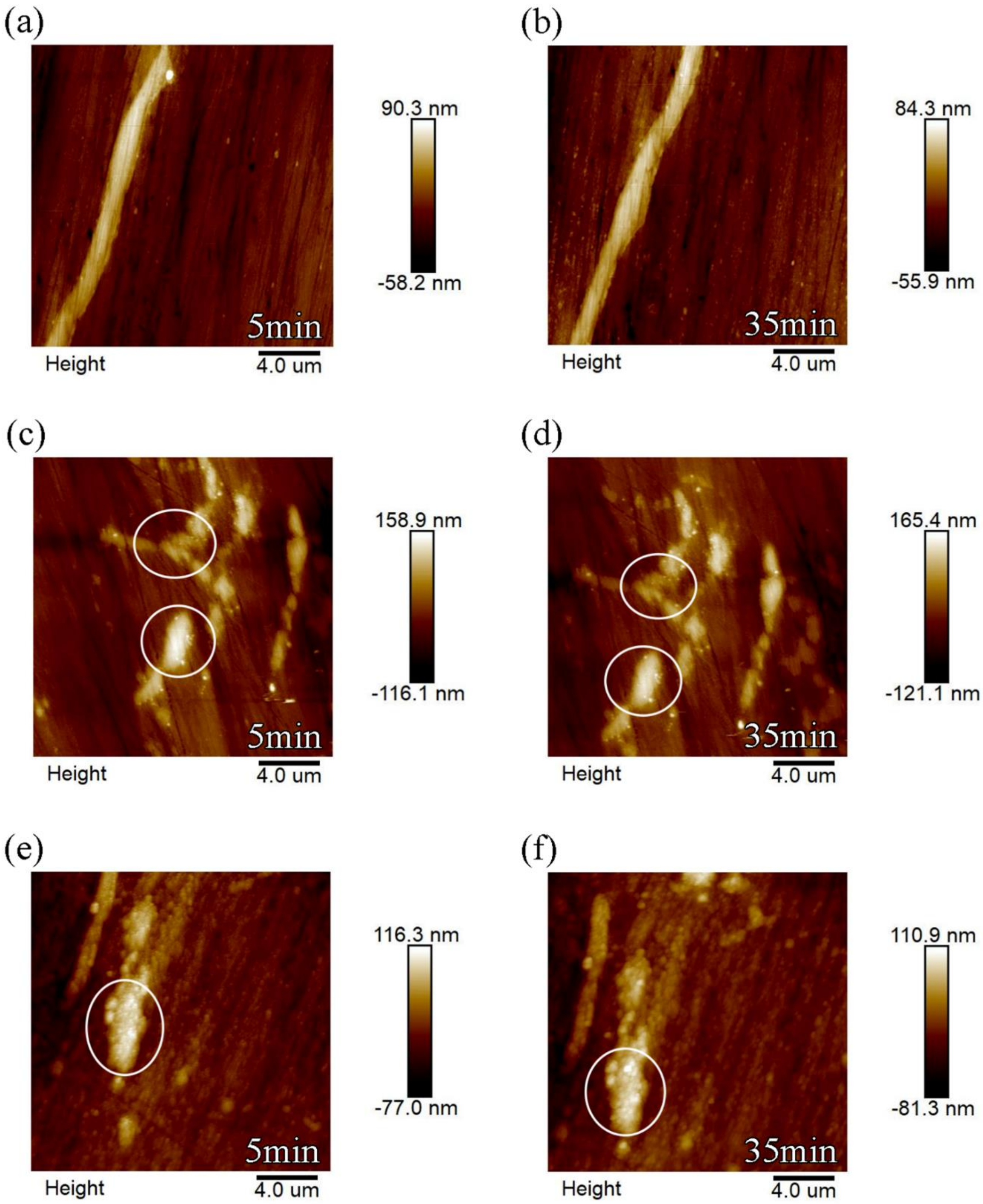

Figure 4. Corrosion morphologies in-situ observed by EC AFM after immersion in 0.1 mol/L NaCl solution for 5 min and 35 min (a)(b) semi-continuous as-cast alloy, (c)(d) transverse section of extruded alloy, (e)(f) longitudinal section of extruded alloy.

Fig. 5 shows the SEM micrographs of the AZ91 alloy with 1.0% (La, Ce) MM addition under different condition after immersion in 3.5%wt NaCl solution for 10 min. From the Figs. 5 (a) and (b), it is evident that localized corrosion commenced with dissolution at interface between the several Al_4(La, Ce) phase and Mg matrix (circle-marked places), corrosion is particularly severe at the interface between the β-$Mg_{17}Al_{12}$ phase and the matrix.

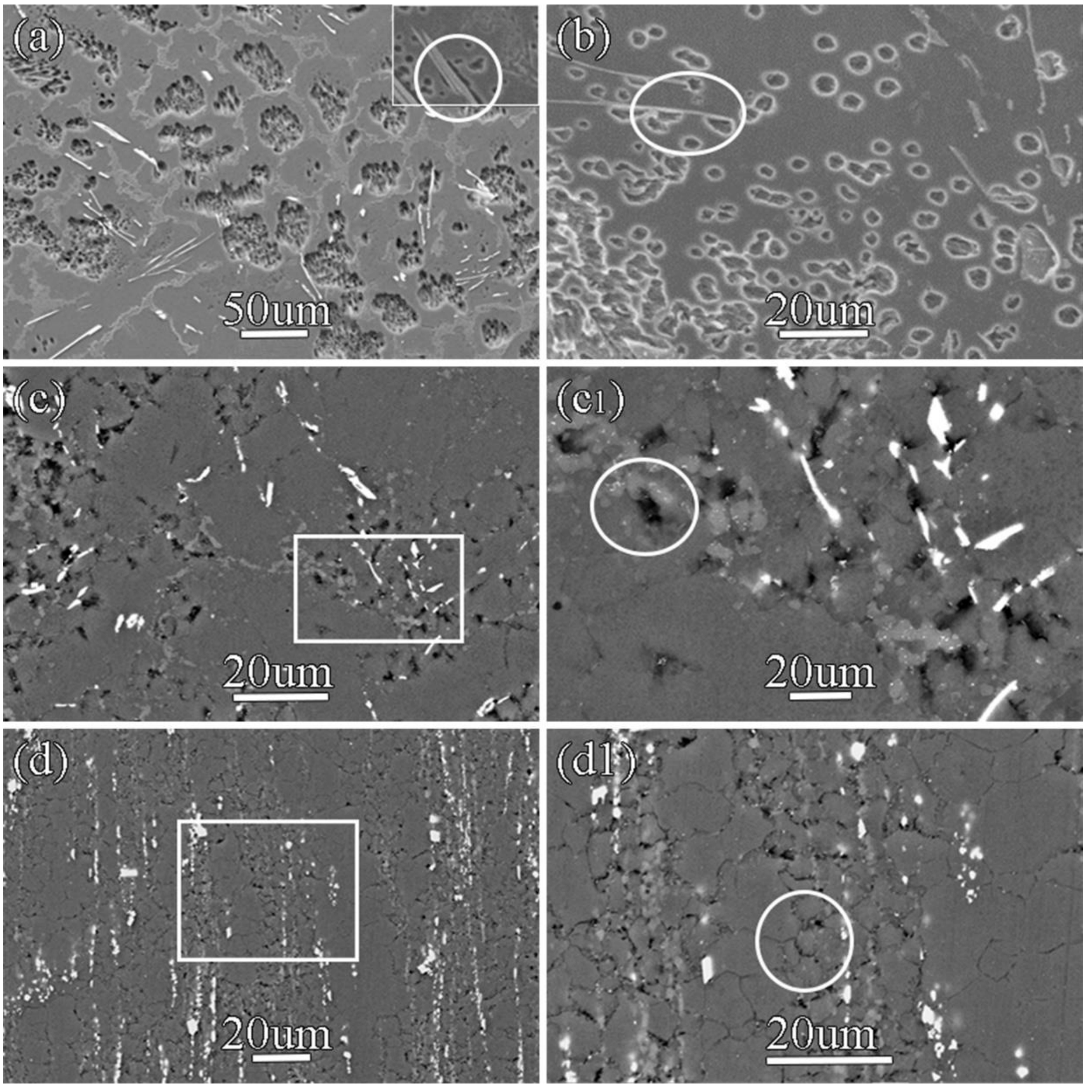

Figure 5. Corrosion morphologies observed by SEM after immersion in 3.5%wt NaCl solution for 10 min (a) semi continuous as-cast alloy, (b) homogenization treatment alloy, (c) transverse section of extruded alloy, (c1) high magnification of (c), (d) longitudinal section of extruded alloy, (d1) high magnification of (d).

This suggests that β-$Mg_{17}Al_{12}$ phase is an effective cathode and Al_4(La, Ce) phase is a weak cathode. The corrosion morphologies are observed in the transverse section of the extruded Mg alloy (Figs. 5 (c) and (d)). The corrosion morphology is mainly pitting corrosion along grain boundaries, which is different from the localized corrosion morphology on the Mg matrix before extrusion. In addition, the surface of the transverse section exhibits micro-galvanic corrosion morphology which was driven by the cathode phases of several Al_4(La, Ce) and the β-$Mg_{17}Al_{12}$ (square-marked in Fig. 5(c) and circle-marked places in Fig. 5(c1)). For the longitudinal section, the corrosion morphologies are characterized by streamline parallel to extrusion direction (square-marked in Fig. 5(d)). From the higher magnification image (Fig. 5(d1)), it can be clearly seen that the corrosion mainly occurs at the grain boundaries of the recrystallized grain (Fig. 5(d) and (d1)), which is probably related to the distorted lattice letting the atom more susceptible to corrosion [23]. Because the recrystallized grain distributes along the extrusion direction and their size is so small, corrosion streamlines form in the longitudinal section. Similar phenomenon was reported by Ji [24], they found parallel streamline of shear stripe in the longitudinal section of the extruded Mg-5Ca-2.5Nd alloy, which makes obvious corrosion streamline in the corrosion process. In addition, they discussed the effect of grain size on the corrosion resistance of Mg-5Ca-2.5Nd alloy, and found that the smaller the grain size, the better the corrosion resistance. But corrosion resistance was also affected by the uniformity of grain size. Corrosion resistance on the longitudinal section of the alloy was lower because the grain size was obviously uneven. It is different from the observation results by EC AFM, micro-galvanic corrosion has been found in the longitudinal section from the corrosion morphology observed by SEM (Fig. 5(d1)). Corrosion attacks the matrix adjacent to the β-$Mg_{17}Al_{12}$ phase. The decrease in the size of the β-$Mg_{17}Al_{12}$ phase reduced the area of the cathode of the micro-galvanic coupling. This is beneficial to improve the corrosion resistance of the extruded alloy. For the Al_4(La, Ce) phases, the changes in size and relative potential difference have no remarkable effect on their micro-galvanic corrosion behavior. In other words, the cathode effect of the Al_4(La, Ce) phases is weak before and after extrusion in spite of the relatively higher relative potential difference measured.

4. CONCLUSIONS

1. The effect of hot extrusion on the microstructure of AZ91 alloy with 1.0% (La, Ce) MM addition was investigated. The grains are obviously refined and the size of β-$Mg_{17}Al_{12}$ phase and Al_4(La, Ce) phase in alloy is reduced to below 1μm or 1-2μm after extrusion. The grain size is uniform and the intermetallic phases disperse in the transverse section. The intermetallic phases present a strip distribution along the extrusion direction in the longitudinal section of the extruded alloy.
2. The relative potential difference of the intermetallic phases was influenced by extrusion process. The intermetallic phases in the longitudinal section of the extruded alloy have relatively higher potential difference. The relative potential difference between the β-$Mg_{17}Al_{12}$ phase and matrix is 300-370 mV and the value of Al_4(La, Ce) phase reaches 410-440 mV or 470-520 mV.
3. The microstructure of extruded alloy has great influence on the corrosion behavior. The size decreasing and elevated relatively potential difference of Al_4(La, Ce) phase has no remarkable effect on the micro-galvanic corrosion behavior of the extruded alloy, Al_4(La, Ce) phase is still a weak cathode. The micro-galvanic corrosion can be driven by the effective cathode of β-$Mg_{17}Al_{12}$ phase and individual Al_4(La, Ce) phase in the transverse section, whose corrosion morphology is pitting corrosion. The corrosion morphology in the longitudinal section is mainly influenced by extrusion direction, it is characterized by corrosion streamline along the extrusion direction, the corrosion mostly occurs at the

grain boundaries of the recrystallized grain.

ACKNOWLEDGEMENTS
This work was supported by the National Natural Science Foundation of China projects under Grant No.51961029 and No.51531007.

References

1. G. L. Song, M. Liu, Z. M. Shi, F. Y. Cao, and M. S. Dargusch, *Adv.Eng. Mater.*, 4 (2015) 400.
2. H. E. riedrich and B. L. Mordike, Magnesium Technology Metallurgy, Design Data, Applications. 2006, Berlin; New York: Springer.
3. I.J. Polmear, Magnesium and Magnesium Alloys ASM Specialty Handbook.1999, ASM International: Materials Park.
4. N. N. Aung and W. Zhou, *Corros. Sci.,* 52 (2010) 589.
5. Z.M. Li, D.Q. Wan, Y. Huang, S.T. Ye and Y.L. Hu, *J. Magnes. Alloy*., 5 (2017) 217.
6. J.F. Wang, W.Y. Jiang, Y. Ma, Y. Li and S. Huang, *Mater. Chem. Phys*.,203 (2018) 352.
7. M. Tan, Z. M. Liu and G.F. Quan, *Energy Procedia*,16 (2012) 457.
8. S. K. Guan, S. J. Zhu and L. G. Wang, *T. Nonferr. Metal. Soc*.,17 (2007) 1143.
9. S. M. Masoudpanah and R. Mahmudi, *Mater. Des*., 31 (2010) 3512.
10. D. Orlov, R. George and T. T. Lamark, *Acta Mater*., 59 (2011) 375.
11. L. Chen, C. G. Chen and N. N. Wang, *Rare Metal Mat. Eng*., 44 (2015) 333.
12. N. Birbilis, K. D. Ralston and S. Virtanen, *Corros. Eng., Sci. Technol*., 45 (2010) 224.
13. G. B. Hamu, D. Eliezer and L. Wagner, *J. Alloys Compd*.,468 (2009) 222.
14. A. E. Coy, F. Viejo, P. Skeldon, and G. E. Thompson, *Corros. Sci*., 52(2010)3896.
15. R. Arrabal, B. Mingo, A. Pardo, E. Matykina, M. Mohedano, M. C. Merino, A. Rivas and A. Maroto, *Corros. Sci*., 97 (2015) 38.
16. R. L. Jia, M. Zhang, L. N. Zhang, W. Zhang and F. Guo, *J. Alloys Compd*., 634 (2015) 263.
17. D. B. Blu, J. E. Svensson, L. G. Johansson, M. Rohwerder and M. Stratmann, *J. Electrochem. Soc.*, 151 (2004) 621.
18. M. C. Zhao, M. Liu and G. L. Song, *Corros. Sci*., 50 (2008)1939.
19. R. L. Jia, S. Yu, D. Li, T. Zhang, F. H. Wang, C. Zhong, *J. Alloys Compd*.,778 (2019) 427.
20. Y. Zhu, M.L. Hu, D.J. Wang, H.Y. Xu, Y. W and Z.S. Ji, *Mater. Sci. Technol*., 34 (2018) 876
21. Z. Zeng, N. Stanford and C. H. Davies, *Int. Mater. Rev*., 2 (2018)1.
22. M. F. Hurley, C. M. Efaw, P. H. Davis, J. R. Croteau, E. Graugnard, and N. Birbilis, *Corros.,* 71, (2015)160.
23. T. Zhang, G. Z. Meng, Y. W. Shao, Z. Y. Cui, F. H. Wang, *Corros. Sci*., 53 (2011)2934.
24. X.Y. Ji, Z.H. Han and H. Guo, *Hot Working Technol*., 46 (2017) 104.